ACS Photonics

Letter

pubs.acs.org/journal/apchd5

Enhanced Second-Harmonic Generation by Metasurface Nanomixer and Nanocavity

Pai-Yen Chen,[†,‡] Christos Argyropoulos,[‡,§] Giuseppe D'Aguanno,[∥] and Andrea Alù*[,‡]

[†]Department of Electrical and Computer Engineering, Wayne State University, Detroit, Michigan 48202, United States

[‡]Department of Electrical and Computer Engineering, University of Texas at Austin, Austin, Texas 78712, United States

[§]Department of Electrical and Computer Engineering, University of Nebraska−Lincoln, Lincoln, Nebraska 68588, United States

[∥]Department of Computer Science and Electrical Engineering, University of Maryland, 1000 Hilltop Circle, Baltimore, Maryland 21250, United States

ABSTRACT: We discuss the possibility of largely enhancing the nonlinear second-harmonic generation (SHG) from $\chi^{(2)}$ nonlinear materials using metasurfaces consisting of suitably engineered optical nanoantenna arrays. The proposed setup may increase the SHG conversion efficiency by orders of magnitude, compared to a thin film of $\chi^{(2)}$ nonlinear material of the same thickness. This enhancement is attributed to localized fields at the nanoload, due to the plasmonic resonance of noble-metal nanoantennas, combined with a suitably enhanced photonic local density of states induced by properly coupling two closely spaced metasurfaces to form a nanocavity to enhance SHG. The proposed subwavelength optical device can lead to versatile applications, such as wavelength conversion and wave mixing at the nanoscale.

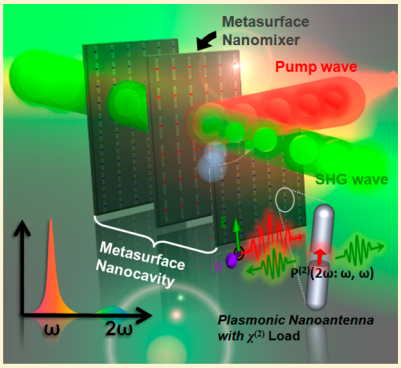

KEYWORDS: *harmonic generation, nanoantennas, plasmonics, nonlinear optics, nano-optics, metasurfaces*

During recent years, there has been a growing interest in extraordinary and anomalous optical responses of noble-metal nanoparticles,[1,2] nanoapertures in metal films,[3,4] and optical metamaterials,[5] taking advantage of strong *light−matter interactions* over nanometer dimensions. This is achievable with extremely localized surface plasmon polariton (SPP) waves. Random and periodic metal clusters[6−8] exhibit a great potential to achieve large local field enhancement, which is particularly important to excite weak optical responses and optical nonlinearities, such as second-harmonic generation (SHG)[9] and surface-enhanced Raman scattering (SERS).[10] Manipulation of optical information by SPP waves at subwavelength scale has been extensively studied in the realm of linear optics, giving rise to a variety of plasmonic optical devices, such as optical nanoantennas,[11−16] plasmonic waveguides and cavities,[2,17] super lenses,[18−20] cloaking,[21−23] and optical nanocircuitry.[24] Increased attention has been recently devoted to enhanced nonlinear optical responses of plasmonic nanostructures composed of single[6] or multiple nanoparticles.[25] Palomba and Novotny[26] have experimentally demonstrated that, by reducing the separation between a pair of noble-metal nanoparticles to just a few nanometers, the intensity of the degenerate four-wave mixing (FWM) signal ($\omega_{FWM} = 2\omega_1 - \omega_2$) can be enhanced by several orders of magnitude, resulting from the strong localized electric field at the nanojunction of a dimer nanoantenna and the enhanced $\chi^{(3)}$ nonlinearity at the metal surface. This leads to a highly confined, coherent, and frequency-tunable local photon source. More recently, theoretical and experimental works have also demonstrated that optical nonlinearities can be significantly enhanced by plasmonic resonances, which sensitively depend upon geometrical variations in plasmonic particles,[25−31] the local environment, and the polarization of the impinging wave. Such controllable, dramatic local field enhancement is expected to be beneficial in a great number of nonlinear optics applications, such as wave mixing or wavelength conversion at the nanoscale,[26] phase-conjugating perfect lenses,[32] high-resolution fluorescence imaging,[26] two-photon microscopy, optical switching,[12,13,26] and nonlinear magnetic optical metamaterials.[31] In these applications, lasers with tunable wavelength, high peak intensities (sometimes larger than 1−10 GW/cm^2), and short pulse duration (∼200 fs) and repetition rate (76 MHz) are usually used to excite the nonlinear response of nanoparticles.[25,26]

In the literature, artificially synthesized $\chi^{(2)}$ nonlinear composite materials have received relatively less attention compared to $\chi^{(3)}$ nonlinear composite materials, since the former need to rely on noncentrosymmetric geometries lacking the inverse symmetry. For this reason, the majority of work on nonlinear composite materials[7,26−29] has been focused on third-order nonlinearities in metal- and semiconductor-doped dielectric materials, in which the nonlinearity arises primarily from the inclusions' strong local $\chi^{(3)}$effects. However, with the

Received: April 17, 2015
Published: July 13, 2015

DOI: 10.1021/acsphotonics.5b00205
ACS Photonics 2015, 2, 1000−1006

rapid progress in nanofabrication and nanophotonics, the design and synthesis of inclusions with noncentrosymmetric geometries became possible, and experimental evidence of SHG has been found in nanodimensional split-ring resonators (SRRs),[31] asymmetric nanoparticles,[30] core−shell nanocomposites,[10] and metasufaces.[33,34] Second-order nonlinear composites, however, need to either implement the design of complex noncentrosymmetric inclusions with a weak nonlinearity induced by asymmetric geometries[30] or cover $\chi^{(2)}$ nonlinear nanoparticles with plasmonic coatings, which, however, exhibit a narrow frequency range of surface plasmon resonance.[10] These drawbacks, in general, restrict their practical application but can be advantageous for other applications, such as nanolasing. In this work, we propose a basic approach to induce strong second-order nonlinear effects based on plasmonic field enhancement sustained by ultrathin metasurfaces composed of arrays of plasmonic nanoantennas, loaded with $\chi^{(2)}$ nonlinear optical materials (NOM) at the dipole's gap (Figure 1b). Interestingly, the considered inclusions are simple nanorods, with inherent symmetry, but they are loaded by materials with $\chi^{(2)}$ response.

The optical metasurface is somewhat the optical equivalent of a radio frequency (RF) mixer composed of a conductive antenna and a Schottky diode load.[35] It is relevant to underline important differences between these two concepts. First, nonlinear loads at RF are generally controlled by the *bias voltage* at their terminals, and therefore their functionalities are independent of the gap size or the distance between their terminals. At optical frequencies, instead, one may consider nonlinear nanoloads with non-negligible second-order nonlinearity, which is directly related to the *local field* amplitude at the nanogap. The nanoantennas' plasmonic features can lead to large local field enhancement at the nanometer gap in the optical regime, based on which the nonlinear properties of nanoloads may be drastically enhanced and controlled with relatively low impinging optical intensities. As a result, the structure proposed here provides a flexible design to realize efficient three-wave mixing at design frequencies, selected by tuning the geometry or load material (and accordingly the resonance frequency) of nanoantennas in the realm of optical nanocircuits.[24] Here the SHG process, which is considered as a representative example to tackle $\chi^{(2)}$ effects, will be studied. Despite the small volume of $\chi^{(2)}$ NOM, the proposed metasurface-formed nanomixer or optical frequency nanomultiplier can generate SHG waves with remarkably high conversion efficiency compared to the equivalent volume of a conventional bulk nonlinear material.[36] Moreover, since the nanoantennas are quite selective to frequency, the metasurface is highly reflective only at its resonance frequency, while being almost transparent for frequencies that are away from the resonance frequency. Motivated by such intriguing scattering properties, we also explore the design of a nanocavity formed by two additional metasurfaces, whose coupling can further boost the local photonic density of states and allow further nonlinearity enhancement. The pump wave at the fundamental frequency ω may in fact penetrate the nanocavity because it is transparent (except at the SHG frequency), inducing second-harmonic waves generated from the nonlinear metasurface, whose magnitude can be then further enhanced by an external nanocavity, and forming an efficient localized nonlinear light source, as illustrated in Figure 1a. In the following, we discuss potentials and practical implementation of an optical frequency nanomultiplier formed by integrally stacked plasmonic metasurfaces.

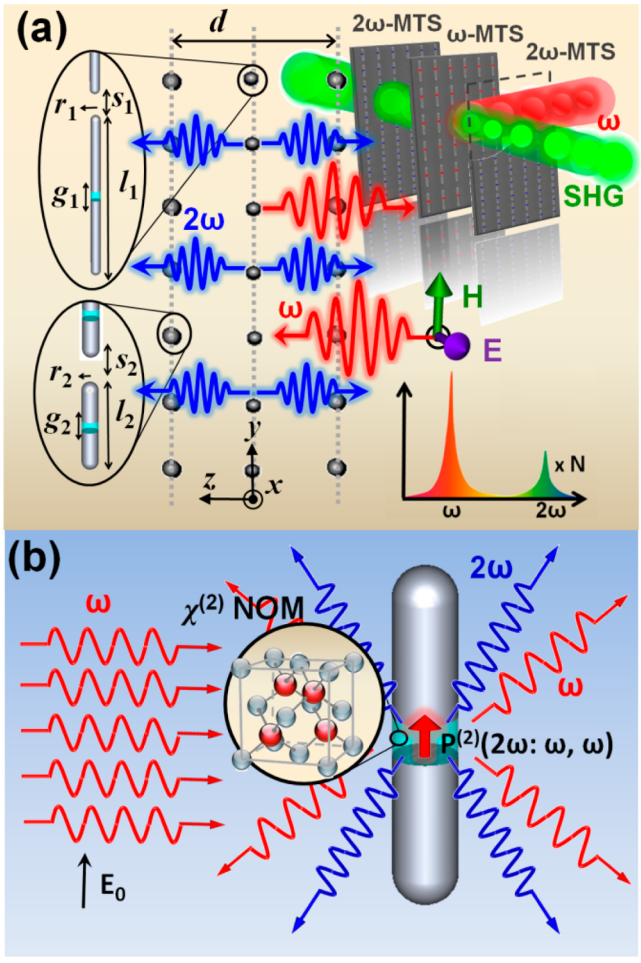

Figure 1. (a) Design and operation principle of the proposed system, consisting of a metasurface (MTS) nanomixer located at the center of a metasurface nanocavity. (b) A single silver nanoantenna loaded with $\chi^{(2)}$ nonlinear optical material ($\chi^{(2)}$-NOM) induces a nonlinear radiative dipole in the load region.

In the linear regime, the main extinction resonances of the proposed metasurface arise from the collective Rayleigh dipolar scattering of the nanoantennas, based on which a reflection peak depends on the plasmon oscillation length of the nanoantennas. An individual nanoantenna in our design is assembled by a pair of silver nanowires conjoined with a nanoparticle load, whose permittivity in the linear region is assumed to be $\varepsilon_L = 2.25\varepsilon_0$, where ε_0 is the permittivity of free space. The relative permittivity of silver nanowires is described by the Drude-dispersion model obtained from experimental data as $\varepsilon_{AG} = \varepsilon_\infty - \omega_p^2/[\omega(\omega - j\gamma)]$, with $\omega_p/2\pi = 2175$ THz, $\gamma/2\pi = 4.35$ THz, and $\varepsilon_\infty = 5$.[37] For a single nanoantenna with a resonant peak at 265 THz in free space, the physical dimensions are $l_1 = 180$ nm, $r_1 = 5$ nm, and $g_1 = 10$ nm (Figure 1a). Figure 2a shows the magnitude and phase of polarizability α (normalized by $6\pi\varepsilon_0/k_0^3$) for an individual nanoantenna in the linear regime, obtained with full-wave simulations.[38] The inset of Figure 2a presents the corresponding far-field radiation pattern, showing typical dipolar radiation. From Figure 2a, a sharp peak in the magnitude of polarizability and a corresponding 180 deg phase shift are observed at the nanoantenna resonance frequency, accompanied by a very

DOI: 10.1021/acsphotonics.5b00205
ACS Photonics 2015, 2, 1000−1006

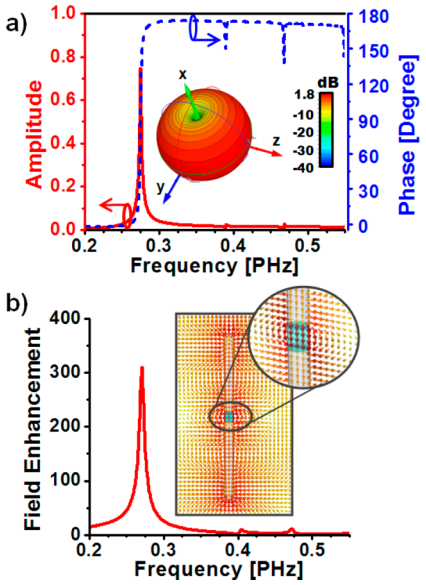

Figure 2. (a) Magnitude and phase of polarizability. The far-field radiation pattern is shown in the inset. (b) Local field enhancement and electric near-field distribution of an individual nanoantenna in the linear regime, showing resonant plasmonic features and continuity of the displacement current across the nanoload.

strong local field enhancement due to the plasmonic resonance (Figure 2b). For this dimer-type nanoantenna, the scattering is sensitively dependent on the polarization of the impinging wave and the optical interaction with the plasmonic nanoantenna and is strongest when the polarization is parallel to the dipole-arm axis. We note that a polarization-independent metasurface may be preferable in practical applications, especially considering that many optical crystals provide cross-polarized nonlinear response. A more isotropic effect can be straightforwardly realized by designing nanoantennas that resonate along both polarizing axes, for example with a cross-dipole design.

Figure 3 shows the variation in reflection for a metasurface composed of a planar array of nanoantennas with periods a_{x1} = a_{y1} = 250 nm (red solid line), calculated again using full-wave simulations. A reflection peak is observed around an individual nanoantenna's resonant frequency, which is slightly shifted to $\omega/2\pi$ = 275 THz due to the coupling with neighboring

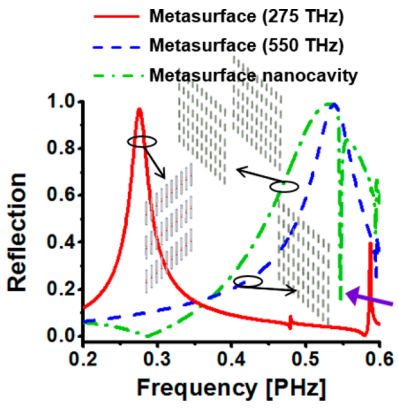

Figure 3. Reflection coefficients for metasurfaces with operation frequencies of 275 THz (red solid line) and 550 THz (blue dashed line) and for the metasurface nanocavity with a narrowband transmission at 550 THz (green dash-dot line).

nanoantennas. This reflection peak is associated with a small value of Re$[\alpha^{-1}]$, related to the *inclusion* resonance (the metasurface resonant condition is Re$[\alpha^{-1}]$ = Re$[C]$, where C is the interaction constant[39−43]). This is different from the *lattice* resonance caused by the coupling with the entire lattice stemming from its periodic features,[39−43] which typically exists in arrays with periods comparable to the transverse wavenumber of impinging light. A metasurface aimed to resonate at the SHG frequency ($2\omega/2\pi$ = 550 THz) can be designed by varying the length of the dipole-arm or choosing alternative nanoloads. Fixing all material properties, the geometric parameters for such a 2ω-metasurface are l_2 = 70 nm, r_2 = 10 nm, and g_2 = 15 nm. Figure 3 also shows the reflection of a 2ω-metasurface (blue dashed line), showing a reflection peak only at 2ω. However, by combining a pair of 2ω-metasurfaces with a proper separation distance d = 265 nm, a nanocavity can be formed, with a narrow-bandwidth resonant transparency associated with a high quality-factor at 2ω (green dash-dot line of Figure 3), analogous to the tunneling frequency in a Fabry−Perot cavity. As expected from electromagnetic reciprocity, if a 2ω-light source is located at the nanocavity center, the SHG emission will be highly amplified due to the large local density of states.

Next, we investigate enhanced SHG by a nanoantenna metasurface with $\chi^{(2)}$ nanoparticle loads. The SHG process, i.e., converting the frequency of light from ω to 2ω, is a degenerate three-wave mixing ($2\omega = \omega + \omega$) procedure. Here we assume that the pump is a normally incident transverse electric (TE) wave with electric field polarized parallel to the nanoantenna axis $\mathbf{E}_{inc} = \hat{x}E_0 \exp[j(\omega t - k_0 z)]$. Following our recently proposed homogenization model for linear metasurfaces,[39−43] we propose here a dynamic analytical model for nonlinear metasurfaces, considering the interaction and coupling of neighboring dipoles, as well as nonlinear wave mixing. For our geometry, it is safe to ignore other multipolar radiation orders, because their effects are negligible. Since the nanoantenna length is subwavelength at the frequency of operation, $\omega/2\pi$ = 275 THz ($l \approx \lambda_0/6$), the collective response of the induced second-order dipole moments in each nonlinear nanoload (see Figure 1b) may be equivalent to a homogeneous surface current sheet, which radiates the SHG wave with a planar wavefront[43] toward both sides of the metasurface. The total averaged second-order polarization related to the local field $\mathbf{E}_{loc}$ at the mixing frequency 2ω is given by[43−45]

$$\mathbf{P}^{(2)}_{NxNy}(2\omega) = \alpha(2\omega)\,\mathbf{E}_{loc}(2\omega) + \beta(2\omega;\,\omega,\,\omega)\,\mathbf{E}_{loc}(\omega)\,\mathbf{E}_{loc}(\omega) \quad (1)$$

where N_x and N_y are positive or negative integers that relate the nanoantenna position and periods a_x and a_y by $x = N_x a_x$ and $y = N_y a_y$, $\alpha(2\omega)$is the polarizability accounting for Rayleigh scattering at frequency 2ω (as calculated in Figure 2a), and $\beta(2\omega{:}\omega,\omega)$ is the hyperpolarizability, accounting for hyper-Rayleigh scattering, and it can be derived from reciprocity as $\beta(2\omega) \approx \chi^{(2)}(\varepsilon_0 \pi r_1^2 g_1)\, f_{rad}(2\omega)\, f_g^2(\omega)$,[11,44] where the dimensionless factor $f_{rad}(2\omega)$ = 1 considers the enhancement of antenna radiation at 2ω and the dimensionless factor $f_g(\omega)$ = 308.5 considers the local field enhancement at the nanogap compared to the macroscopic external field; these values are obtained from linear full-wave simulations based on the finite integration technique[38] monitoring the fields at the nanogap. At the mixing frequency 2ω, considering the coupling among nanoantennas, we can write eq 1 as

DOI: 10.1021/acsphotonics.5b00205
ACS Photonics 2015, 2, 1000−1006

$$\mathbf{P}^{(2)}_{N'xN'y}(2\omega) = \alpha(2\omega)\,\mathbf{E}_{\mathrm{loc}}(2\omega) + \beta(2\omega;\,\omega,\,\omega)\,\mathbf{E}_{\mathrm{loc}}(\omega)\,\mathbf{E}_{\mathrm{loc}}(\omega)$$
$$= \alpha(2\omega)\sum_{(N_x,N_y)\neq(N'x,N'y)}\mathbf{G}^{2\omega}(\mathbf{r}_{N_xN_y}-\mathbf{r}_{N'x,N'y})\frac{\mathbf{P}^{(2)}_{N'x,N'y}(2\omega)}{\varepsilon_0}+$$
$$\beta(2\omega;\,\omega,\,\omega)$$
$$\times\left[\mathbf{E}_{\mathrm{inc}}(\omega)+\sum_{(N_x,N_y)\neq(N'x,N'y)}\mathbf{G}^{\omega}(\mathbf{r}_{N_xN_y}-\mathbf{r}_{N'x,N'y})\frac{\mathbf{P}^{(1)}_{N'x,N'y}(\omega)}{\varepsilon_0}\right]^2 \tag{2}$$

where $\mathbf{G}(\mathbf{r}_{lmn})$ is the electric dyadic Green's function:[39−43]

$$\mathbf{G}(\mathbf{r}_{N_xN_y}) = (\nabla\nabla + k^2\bar{\bar{\mathbf{I}}})\frac{e^{-jk_0r}}{4\pi r} \tag{3}$$

After some algebraic manipulation, we may simplify eq 2 into

$$\mathbf{P}^{(2)}_{00}(2\omega) = \hat{x}P^{(2)}_{00}(2\omega)$$
$$= \frac{\beta(2\omega:\,\omega,\,\omega)}{1-\varepsilon_0^{-1}\alpha(2\omega)C^{2\omega}}\left[\frac{\mathbf{E}_{\mathrm{inc}}(\omega)}{1-\varepsilon_0^{-1}\alpha(\omega)C^{\omega}}\right]^2$$
$$= \beta(2\omega:\,\omega,\,\omega)\,L(2\omega)\,L(\omega)\,L(\omega)\,\mathbf{E}_{\mathrm{inc}}(\omega)\,\mathbf{E}_{\mathrm{inc}}(\omega) \tag{4}$$

where C is the interaction constant, which relates the fields induced by the infinite array of dipoles around the unit cell under consideration to the local field at the origin, and L is the local field correction factor,[43] given by

$$C^{\omega'} = \sum_{(N_x,N_y)\neq(0,0)}\mathbf{G}^{\omega'}(\mathbf{r}_{N_xN_y})\cdot\hat{x}\cdot\hat{x},$$
$$L(\omega') = [1-\varepsilon_0^{-1}\alpha(\omega')C^{\omega'}]^{-1} \tag{5}$$

where ω' is an arbitrary frequency. The averaged surface current at the $z = 0$ plane sustained by the collective nonlinear dipole moments $\mathbf{P}^{(2)}$ is given by

$$\mathbf{J}^{\mathrm{SHG}}_{\mathrm{av}} = \hat{x}J^{\mathrm{SHG}}_{\mathrm{av}} = \frac{j2\omega\mathbf{P}^{(2)}_{00}(2\omega)}{d_xd_y} =$$
$$= \hat{x}\frac{j2\omega}{d_xd_y}\beta(2\omega:\,\omega,\,\omega)\,L(2\omega)\,L(\omega)\,L(\omega)\,E_0(\omega)\,E_0(\omega) \tag{6}$$

Since this ultrathin metasurface has a negligible thickness, we should consider *phase matching* only for the tangential wave vector parallel to the metasurface $k_x^{2\omega} = 2k_x^{\omega}$, which is, however, irrelevant for normal incidence. For oblique illumination with angle of incidence $\theta_{\mathrm{in}} = \sin^{-1}(k_x/k_0)$, the SHG wave will propagate with an angle $\theta_{\mathrm{SHG}} = \sin^{-1}(2k_x/2k_0) = \theta_{\mathrm{in}}$ in order to meet the phase-matching condition. Moreover, due to the extreme thinness of the metasurface, the SHG light will radiate equally on both sides of the metasurface, as illustrated in Figure 1a, and the electric fields at 2ω are given by

$$\mathbf{E}^{\mathrm{SHG},\pm} = -\frac{J^{\mathrm{SHG}}_{\mathrm{av}}\eta_0}{2}\exp[\mp j(2k_0)z]\hat{x} \tag{7}$$

where η_0 is the free-space impedance. The SHG scattering coefficient $\sigma^{\mathrm{SHG}}_{\mathrm{sca}}$ is defined as the ratio of the amplitude of the forward and backward propagating SHG waves to the incident electric field:

$$\sigma^{\mathrm{SHG}}_{\mathrm{sca}} = -\frac{1}{2}\frac{j(2\omega)}{d_xd_y}\eta_0\beta(2\omega:\,\omega,\,\omega)\,L(2\omega)\,L(\omega)\,L(\omega)\left[\frac{2I_0}{c\varepsilon_0}\right]^{1/2} \tag{8}$$

where I_0 is the power density of the pump wave at the fundamental frequency ω. As expected, the forward and backward propagating SHG waves have the same magnitude, since an ultrathin source, as an infinite two-dimensional current sheet, equally radiates for symmetry toward both sides. Therefore, the efficiency η of power conversion is given by

$$\eta = 2\,|\sigma^{\mathrm{SHG}}_{\mathrm{sca}}|^2 \tag{9}$$

From eqs 8 and 9, we note that the SHG conversion efficiency is almost linearly proportional to the input power, as the nonlinear wave mixing occurs at an ultrathin surface. We consider now a realistic scenario: a pump wave with frequency around the metasurface resonance frequency and a reasonably high power density $I_0 = 1$ GW/cm^2. For high-intensity laser pumping, a pulsed operation is required to avoid heating issues: a nanoload with linear permittivity $\varepsilon_L = 2.25\varepsilon_0$ and second-order susceptibility $\chi^{(2)} = 25$ pm/V (i.e., $\chi^{(2)}$ is on this order for some III−V compounds, such as GaAs and $CdGeAs_2$[44]). Figure 4 shows the SHG conversion efficiency over the spectrum for

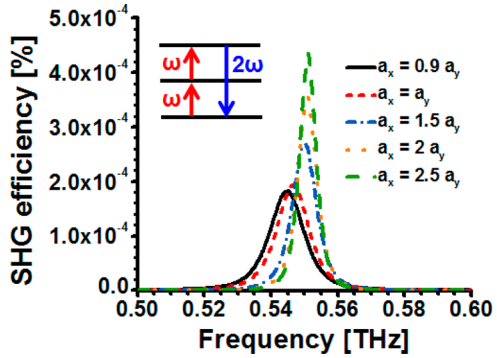

Figure 4. Spectrum of SHG conversion efficiency for a ω-metasurface with different periods.

this nanoantenna-formed nanomixer with different periods. A narrowband SHG peak with a conversion efficiency $\eta^{\mathrm{SHG}} = 4.36 \times 10^{-4}$% is obtained for $a_x = 250$ nm and $a_y = 2.5a_y$. This value is quite striking when compared to the SHG conversion efficiency of a bulk NOM film[46] with the same thickness and material properties, which is calculated as 1.16×10^{-7}%. This large enhancement ($\sim 10^3$ order) is mainly attributed to the nanoantenna plasmonic resonance obtained around the pump frequency. It is noticeable that quenching effects are important in such a periodic structure.[39,40,43] A larger spacing in the $\hat{x}$ direction ensures a stronger resonance of the entire array, due to decreased coupling in the direction of polarization of the electric field, providing optimal SHG conversion efficiency. This effect can be observed in Figure 4, in which, counter-intuitively, a sparser metasurface provides improved resonant properties despite the reduced concentration of nonlinear nanoparticles. However, it is noted that when the period becomes too large (i.e., $a_x \geq \lambda_0$), higher-order Floquet modes may come into play, and undesired side lobes arise in the radiation pattern of the array, implying that power is coupled to additional plane waves carried by higher-order Floquet modes.

DOI: 10.1021/acsphotonics.5b00205
ACS Photonics 2015, 2, 1000−1006

In this scenario, our homogenization model requires modifications, as detailed in ref 43. We have verified that in all geometries considered in this paper the assumption of a homogeneous surface neglecting the local granularity of the surfaces is well supported by full-wave simulations, in agreement with our findings in ref 47.

In order to further increase the SHG conversion efficiency, we employ the previously designed metasurface nanocavity (Figure 3) to boost the SHG occurring on the metasurface nanomixer (nanomultiplier) located at the nanocavity center. The nanocavity design can be understood in terms of electromagnetic reciprocity. Provided that the cavity length is properly chosen, an external source can induce a strong electric field at the cavity center. By reciprocity, reversing the excitation condition by placing a localized light source at the cavity center generates strong light emission out of the cavity. Figure 5a

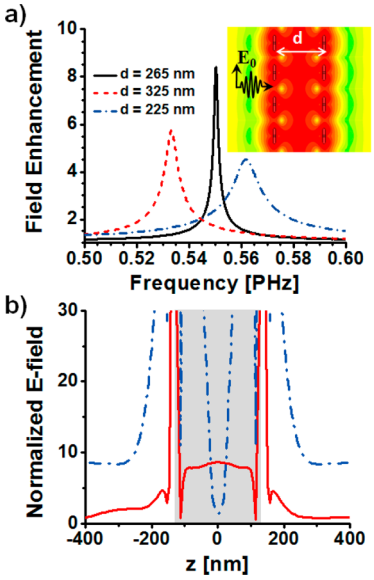

Figure 5. (a) Field enhancement at the center of the nanocavity formed by two 2ω-metasurfaces. (b) Distributions of the normalized *E*-field inside and outside the nanocavity for an external excitation light (red solid line) and the reciprocal case: periodic arrays of dipoles in the middle of a cavity (blue dash-dot line); the shadowed zone is consistent with the nanocavity length.

shows the field enhancement at the cavity center for different nanocavity lengths. The maximum electric field amplification obtained with an optimal cavity length of 265 nm is also verified from the electric field distribution in the inset of Figure 5a. Figure 5b shows the distribution of normalized field strength for external sources propagating from right to left across the nanocavity (red solid line) and compares it with the radiation from a dipole at the nanocavity center (blue dash-dot line). The results show a good agreement in terms of field enhancement. When a nonlinear metasurface resonant at ω is placed in the middle of a cavity formed by two metasurfaces resonant at 2ω, which are effectively transparent to the external pump wave, the SHG wave radiated by the nanomultiplier may be further amplified by the nanocavity to support bursts of narrowband photons. This frequency-selective transparency window is arguably the most important advantage of the proposed metasurface nanocavity. Figure 6 shows the comparison of the SHG conversion efficiency for a nanomultiplier with and without the nanoscale optical cavity. With

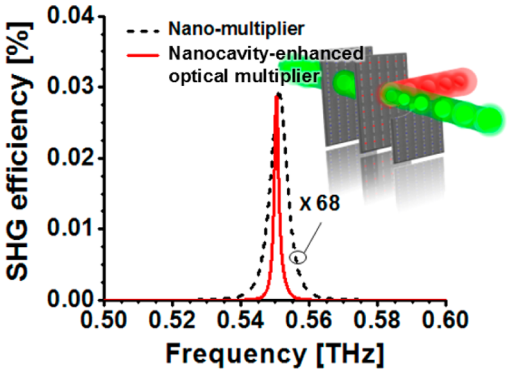

Figure 6. SHG conversion efficiency for the proposed stack of three metasurfaces, forming a nanomultiplier and a nanocavity similar to the setup of Figure 1a. The SHG conversion efficiency for a single nanomultiplier in Figure 4 is also plotted (magnified by 68 times) for comparison.

the nanocavity enhancement, 68 times enhancement is obtained in SHG conversion efficiency, together with a much narrower bandwidth compared to a single nanomixer. The "comb-like" spectrum and the high conversion efficiency are ideal for various nanophotonic applications that require localized nonlinear light sources. It is surprising that the overall SHG conversion efficiency may reach 0.03%, which is around 320 times the SHG's conversion efficiency of 9.4×10^{-5}% of a bulk NOM with thickness comparable to the device length ($d + 2r_2$ = 285 nm). This silver metasurface device can also be tailored to a variety of other nonlinear optics applications. Of particularly interest would be the sum or difference frequency generation $\mathbf{P}^{(2)}(\omega_3;\omega_1,\pm\omega_2)$ or phase conjugation $\mathbf{P}^{(3)}(\omega;\omega,\omega,-\omega)$ for time-reversal applications.[32]

CONCLUSIONS

To conclude, we have proposed a planar nanodevice to enhance optical nonlinearities composed of silver nanoantenna metasurfaces and nonlinear nanoparticle loads, taking advantage of combined resonances of plasmonic nanoantennas in the infrared and visible region. We have shown that a nanocavity formed by two frequency-selective metasurface mirrors can further significantly boost the SHG wave due to the enhanced local density of states in the region enclosed by the two surfaces. This nanocavity-enhanced optical multiplier based on nonlinear metasurfaces may enable various wave mixing and wavelength conversion applications at the nanoscale, paving the way for near-field imaging and spectroscopy, chemical sensing, localized photon sources, and active photonic and plasmonic nanodevices.

AUTHOR INFORMATION

Corresponding Author

*E-mail (A. Alù): alu@mail.utexas.edu. Tel: +1.512-471-5922. Fax: +1-512-471-6598.

Notes

The authors declare no competing financial interest.

ACKNOWLEDGMENTS

This work was partially supported by the U.S. Air Force Office of Scientific Research with grant No. FA9550-14-1-0105 and grant No. FA9550-13-1-0204, the Welch Foundation with grant

DOI: 10.1021/acsphotonics.5b00205
ACS Photonics 2015, 2, 1000−1006

No. F-1802, and the Office of Naval Research with MURI grant No. N00014-10-1-0942.

REFERENCES

(1) Takahara, J.; Yamagishi, S.; Taki, H.; Morimoto, A.; Kobayashi, T. Guiding of a one-dimensional optical beam with nanometer diameter. *Opt. Lett.* **1997**, *22*, 475−457.

(2) Sweatlock, L. A.; Maier, S. A.; Atwater, H. A.; Penninkhof, J. J.; Polman, A. Highly confined electromagnetic fields in arrays of strongly coupled Ag nanoparticles. *Phys. Rev. B: Condens. Matter Mater. Phys.* **2005**, *71*, 235408.

(3) Alù, A.; Engheta, N. Theory of linear chains of metamaterial/plasmonic particles as subdiffraction optical nanotransmission lines. *Phys. Rev. B: Condens. Matter Mater. Phys.* **2006**, *74*, 205436.

(4) Ebbesen, T. W.; Lezec, H. J.; Ghaemi, H. F.; Thio, T.; Wolff, P. A. Extraordinary optical transmission through sub-wavelength hole arrays. *Nature* **1998**, *391*, 667−669.

(5) Argyropoulos, C.; D'Aguanno, G.; Alù, A. Giant second-harmonic generation efficiency and ideal phase matching with a double ϵ-near-zero cross-slit metamaterial. *Phys. Rev. B: Condens. Matter Mater. Phys.* **2014**, *89*, 235401.

(6) Shalaev, V. M. Optical negative-index metamaterials. *Nat. Photonics* **2007**, *1*, 41−48.

(7) Ricard, D.; Roussignol, O.; Flytzanis, C. Surface-mediated enhancement of optical phase conjugation in metal colloids. *Opt. Lett.* **1985**, *10*, 511−513.

(8) Klar, T.; Perner, M.; Grosse, S.; von Plessen, G.; Spirkl, W.; Feldmann, J. Surface-plasmon resonances in single metallic nanoparticles. *Phys. Rev. Lett.* **1998**, *80*, 4249−4252.

(9) Kelly, K. L.; Coronado, E.; Zhao, L. L.; Schatz, G. C. The optical properties of metal nanoparticles: the influence of size, shape, and dielectric environment. *J. Phys. Chem. B* **2003**, *107*, 668−677.

(10) Mattiucci, N.; D'Aguanno, G.; Everitt, H. O.; Foreman, J.; Callahan, J.; Buncick, M. C.; Bloemer, M. J. Ultraviolet surface-enhanced Raman scattering at the plasmonic band edge of a metallic grating. *Opt. Express* **2012**, *20*, 1868−1877.

(11) Pu, Y.; Grange, R.; Hsieh, C. L.; Psaltis, D. Nonlinear optical properties of core-shell nanocavities for enhanced second-harmonic generation. *Phys. Rev. Lett.* **2010**, *104*, 207402.

(12) Chen, P. Y.; Alu, A. Optical nanoantenna arrays loaded with nonlinear materials. *Phys. Rev. B: Condens. Matter Mater. Phys.* **2010**, *82*, 235405.

(13) Chen, P. Y.; Farhat, M.; Alù, A. Bistable and self-tunable negative-index metamaterial at optical frequencies. *Phys. Rev. Lett.* **2011**, *106*, 105503.

(14) Chen, P. Y.; Alù, A. A terahertz photomixer based on plasmonic nanoantennas coupled to a graphene emitter. *Nanotechnology* **2013**, *24*, 455202.

(15) Chen, P. Y.; Farhat, M. Modulatable optical radiators and metasurfaces based on quantum nanoantennas. *Phys. Rev. B: Condens. Matter Mater. Phys.* **2015**, *91*, 035426.

(16) Chen, P. Y.; Alù, A. Subwavelength imaging using phase-conjugating nonlinear nanoantenna arrays. *Nano Lett.* **2011**, *11*, 5514.

(17) Argyropoulos, C.; Chen, P. Y.; D'Aguanno, G.; Engheta, N.; Alu, A. Boosting optical nonlinearities in ϵ-near-zero plasmonic channels. *Phys. Rev. B: Condens. Matter Mater. Phys.* **2012**, *85*, 045129.

(18) Sorger, V. J.; Oulton, R. F.; Yao, J.; Bartal, G.; Zhang, X. Plasmonic Fabry-Pérot nanocavity. *Nano Lett.* **2009**, *9*, 3489−3493.

(19) Fang, N.; Lee, H.; Sun, C.; Zhang, X. Sub-diffraction-limited optical imaging with a silver superlens. *Science* **2005**, *308*, 534.

(20) Shvets, G.; Urzhumov, Y. A. Engineering the electromagnetic properties of periodic nanostructures using electrostatic resonances. *Phys. Rev. Lett.* **2004**, *93*, 243902.

(21) Alù, A.; Engheta, N. Achieving transparency with plasmonic and metamaterial coatings. *Phys. Rev. E* **2005**, *72*, 016623.

(22) Cai, W.; Chettiar, U. K.; Kildshev, A. V.; Shalaev, V. M. Optical cloaking with metamaterials. *Nat. Photonics* **2007**, *1*, 224−227.

(23) Argyropoulos, C.; Chen, P. Y.; Monticone, F.; D'Aguanno, G.; Alù, A. Nonlinear plasmonic cloaks to realize giant all-optical scattering switching. *Phys. Rev. Lett.* **2012**, *108*, 263905.

(24) Engheta, N.; Salandrino, A.; Alù, A. Circuit elements at optical frequencies: nanoinductors, nanocapacitors, and nanoresistors. *Phys. Rev. Lett.* **2005**, *95*, 095504.

(25) Huang, W.; Qian, W.; Jain, P. K.; El-Sayed, M. A. The effect of plasmon field on the coherent Lattice phonon sscillation in electron-beam fabricated gold nanoparticle pairs. *Nano Lett.* **2007**, *7*, 3227−3234.

(26) Danckwerts, M.; Novotny, L. Optical frequency mixing at coupled gold nanoparticles. *Phys. Rev. Lett.* **2007**, *98*, 026104.

(27) Palomba, S.; Novotny, L. Near-field imaging with a localized nonlinear light source. *Nano Lett.* **2009**, *9*, 3801−3804.

(28) Lippitz, M.; van Dijk, M. A.; Orrit, M. Third-harmonic generation from single gold nanoparticles. *Nano Lett.* **2005**, *5*, 799−802.

(29) Hanke, T.; Krauss, G.; Trautlein, D.; Wild, B.; Bratschitsch, R.; Leitenstorfer, A. Efficient nonlinear light emission of single gold optical antennas driven by few-cycle near-infrared pulses. *Phys. Rev. Lett.* **2009**, *103*, 257404.

(30) Canfield, B. K.; Hush, H.; Laukkanen, J.; Bai, B.; Kuittinen, M.; Turunen, J.; Kauranen, M. Local field asymmetry drives second-harmonic generation in noncentrosymmetric nanodimers. *Nano Lett.* **2007**, *7*, 1251−1255.

(31) Klein, M. W.; Enkrich, G.; Wegener, M.; Linden, S. Second-Harmonic Generation from Magnetic Metamaterials. *Science* **2006**, *313*, 502−504.

(32) Pendry, J. B. Time reversal and negative refraction. *Science* **2008**, *322*, 71−73.

(33) Lee, J.; Jung, S.; Chen, P. Y.; Lu, Feng; Demmerle, F.; Boehm, G.; Amann, M.-C.; Alù, A.; Belkin, A. B. Metasurfaces: ultrafast electrically tunable polaritonic metasurfaces. *Adv. Opt. Mater.* **2014**, *2*, 1010.

(34) Lee, J.; Tymchenko, M.; Argyropoulos, C.; Chen, P. Y.; Lu, F.; Demmerle, F.; Boehm, G.; Amann, M. C.; Alù, A.; Belkin, M. A. Giant nonlinear response from plasmonic metasurfaces coupled to intersubband transitions. *Nature* **2014**, *511*, 65.

(35) Malyuskin, O.; Fusco, V. Near field focusing using phase conjugating impedance loaded wire lens. *IEEE Trans. Antenna Propagat.* **2010**, *58*, 2884−2893.

(36) Fischer, G. L.; Boyd, R. W.; Gehr, R. J.; Jenekhe, S. A.; Osaheni, J. A.; Sipe, J. E.; Weller-Brophy, L. A. Enhanced nonlinear optical response of composite materials. *Phys. Rev. Lett.* **1995**, *74*, 1871−1874.

(37) Johnson, P. B.; Christy, R. W. Optical constants of the noble metals. *Phys. Rev. B* **1972**, *6*, 4370−4379.

(38) CST Microwave Studio: http://www.cst.com/.

(39) Belov, P. A.; Simovski, C. R. Homogenization of electromagnetic crystals formed by uniaxial resonant scatterers. *Phys. Rev. E* **2005**, *72*, 026615.

(40) Belov, P. A.; Simovski, C. R. Subwavelength metallic waveguides loaded by uniaxial resonant scatters. *Phys. Rev. E* **2005**, *72*, 036618.

(41) Silveirinha, M. G. Generalized Lorentz-Lorenz formulas for microstructured materials. *Phys. Rev. B: Condens. Matter Mater. Phys.* **2007**, *76*, 245117.

(42) Alù, A. First-principles homogenization theory for periodic metamaterials. *Phys. Rev. B: Condens. Matter Mater. Phys.* **2011**, *84*, 075153l.

(43) Alù, A.; Engheta, N. In *Structured Surfaces as Optical Metamaterials*; Maradudin, A. A., Ed.; Cambridge University Press: Cambridge, 2010.

(44) Boyd, R. W. *Nonlinear Optics*, 3rd ed.; Academic Press: Boston, 2008.

(45) Maki, J. J.; Malcuit, M. S.; Sipe, J. E.; Boyd, R. W. Linear and nonlinear optical measurement of the Lorentz local field. *Phys. Rev. Lett.* **1991**, *67*, 972.

(46) Under perfect phase matching, the SHG efficiency for conversion of power from the fundamental wave to the second-harmonic wave at each point in the crystal can be expressed as η =

DOI: 10.1021/acsphotonics.5b00205
ACS Photonics 2015, 2, 1000−1006

$\tanh^2[\zeta]/\mathrm{sech}^2[0]$, where $\zeta = z/l$ is the normalized distance parameter, z is the distance from the crystal interface, and $l = [2n^2(\omega)\, n(2\omega)\epsilon_0 c^3/I_0]^{1/2}/(\omega\chi^{(2)})$ (here $n(\omega) = n(2\omega) = 1.5$ and $\chi^{(2)} = 25$ pm/V). For more details, please see Chapter 2 in ref 44.

(47) Zhao, Y.; Shi, J.; Sun, L.; Li, X.; Alù, A. Alignment-Free Three-Dimensional Optical Metamaterials. *Adv. Mater.* **2014**, *26*, 1439−1445.

DOI: 10.1021/acsphotonics.5b00205
ACS Photonics 2015, 2, 1000−1006